

# Current studies and future perspectives of *in vivo* synchrotron radiation imaging trials in human patients.

Renata Longo<sup>a,b,\*</sup>

<sup>a</sup> *Department of Physics, University of Trieste, via Valerio 2 3410 Trieste, Italy*

<sup>b</sup> *INFN- sezione di Trieste, via Valerio 2 3410 Trieste, Italy*

---

## Abstract

The coherent and monochromatic x-ray beams available at the synchrotron radiation (SR) laboratories are ideal tools for the development and the initial application of new imaging techniques. In the present paper the history of the clinical studies in k-edge subtraction imaging with SR is summarized, including coronary angiography and bronchography. The results of the recent trial in phase-contrast mammography at Elettra (Trieste, Italy) are discussed, in order to assess the clinical impact of the new imaging modality and the potential interest in its translation to clinical practice. The direct measurement of linear attenuation coefficient obtained during the SR mammography trial is also discussed.

The new program of phase-contrast breast CT under development at Elettra is presented. Recently, 3D breast imaging (tomosynthesis and cone beam breast CT) has been introduced in clinical practice with significant improvement in diagnostic accuracy. The aim of this research is to study the contribution of the phase-contrast to the image quality of breast CT, is introduced.

Increasing the image quality of the x-ray medical images at the level of the results obtained at the SR laboratories is highly desirable, hence the promising techniques for the translation of the phase-contrast imaging to the hospitals are briefly discussed.

**Keywords:** synchrotron radiation, mammography, x-ray phase-contrast imaging, k-edge subtraction radiography

---

\* Corresponding author. Tel.: +39-040-558-3383; fax: +39-040-558-3350; e-mail: renata.longo@ts.infn.it

## 22 1. Introduction

23 It is well known that the object of the first radiograph was the hand of Mrs Rontgen in 1895.  
24 Recently the radiographs of another hand have been published and the contrast mechanism in these  
25 new images is no longer based on x-ray attenuation [1]. Between these images there is more than one  
26 century of physics, radiology and technical developments. In the present paper a recent and fascinating  
27 chapter of this story will be discussed: medical imaging with synchrotron radiation (SR). The new hand  
28 radiographs, obtained using a conventional x-ray generator, may be considered as a result of researches  
29 done in medical imaging with SR and therefore will be discussed in the last section of the present  
30 paper.

31 During the XX century new imaging modalities based on ultrasound and nuclear magnetic resonance  
32 have been developed and are used in clinical practice. However x-ray imaging still has a fundamental  
33 role in medical imaging: digital detectors, tomographic techniques, and image processing tools create  
34 detailed views of the organs inside the human body. On the contrary the technology of x-ray sources  
35 for medical imaging is almost unchanged since the development of the rotating anode x-ray generator  
36 in 1898. One of the main constraints of medical imaging is the short acquisition time. In human body,  
37 there are a number of organs that are moving and that can not be voluntarily stopped. The heart for  
38 instance is an excellent example. The average cardiac frequency is about 60 Hz, consequently in  
39 principle, each radiograph should be acquired in less than 1 sec. Accordingly, x-ray sources suitable for  
40 medical imaging have to produce high flux, putting into consideration the thickness of the human body  
41 and the x-ray attenuation coefficients of its components. The success of the rotating anode in radiology  
42 is due to the capability of the system to obtaining short exposure time and high flux without damaging  
43 the anode surface. On the other side the improvement of x-ray imaging techniques is limited by the  
44 characteristics of the conventional x-ray generator: the wide spectrum which affects dose and contrast,

45 and the relatively large focal spot which introduce blurring and affects the spatial coherence of the  
46 beam. As soon as SR facilities were available for research, the community of the medical imaging  
47 looked at the x-ray SR beam as an ideal tool. The interest for the radiological applications of SR is  
48 based on a number of properties of this radiation and the research in medical imaging with SR may be  
49 split in two periods, the first one is based on the absorption contrast [2] and the second starts with the  
50 advent of the X-ray phase contrast techniques [3].

## 51 **2. The Synchrotron radiation as a quasi-coherent x-ray source for imaging**

### 52 *2.1. Properties of synchrotron radiation*

53 The electromagnetic energy radiated when electrical charges are accelerated, i.e. when their  
54 trajectory is bent in a magnetic field, is called SR. The most common source of SR is the storage ring  
55 that is capable of maintaining charged particles, usually electrons, in a quasi-circular orbit. They  
56 circulate within a high-vacuum cavity, which consists of a series of straight sections connected together  
57 by bends located between the poles of bending magnets. Under the influence of the magnetic field, the  
58 electrons changes direction and an electric dipole radiation is emitted. Due to the relativistic energies of  
59 the electrons, the distribution of the emitted radiation is highly peaked in the forward direction and  
60 each bending magnet therefore emits a fan of highly collimated SR beam. The wide spectrum depends  
61 on electron energy and bending magnet intensity and comprises energies from far infrared up to x-ray.  
62 The energy lost by the electrons to this radiation is recovered by the input of radio frequency power and  
63 the accelerating radio frequency field forces the electrons to be grouped into bunches, accordingly the  
64 radiation has a pulsed structure with a period that is typically a few nanoseconds. Apart from bending  
65 magnets as radiation sources in SR facilities, insertion devices may also be placed in the straight  
66 section of the ring in order to produce beams with specific properties. It is not within the scope of this  
67 paper the discussion of the physics of the SR. A large number of publications are available with  
68 different levels of completeness [2,4].

## 69 2.2. *X-ray imaging with SR*

70 In the field of radiology the ideal beam is tuneable and mono-energetic. This is to avoid beam  
71 hardening effect and to allow the patient-based energy optimization according to the large inter-  
72 individual variability of humans. The broad and continuous spectrum of the SR is so intense that it is  
73 possible to select very tight energy windows to obtain monochromatic x-ray beams suitable for a  
74 radiological examination. The monochromator systems, based on perfect crystals (e.g. Si) in Bragg or  
75 Laue configuration, produce monochromatic beams with high degree of monochromaticity and high flux  
76 that are easily tuneable over wide energy range [4]. Another SR property exploited in x-ray imaging is  
77 its small source size that is defined by the electron bunches dimension in the vertical direction, and by  
78 the collimator aperture at the beamline front-end in the horizontal direction. Moreover due to the  
79 natural collimation of the beam, large source to sample distance are applied (up to 100 m) and still  
80 being able to effectively use all the produced radiation consequently increasing the spatial coherence of  
81 the imaging system.

82 As a first approximation, a coherent source may be depicted as a mono-energetic and point-like  
83 source. The temporal (or longitudinal) coherence describes the energy spectrum and the spatial (or  
84 lateral) coherence describes the source size and the geometry of the imaging system. When a coherent  
85 source is used for imaging, interference and diffraction effects are observed in simple experimental  
86 conditions. For a thorough discussion of the concept of coherence in x-ray see ref [5]. SR beams  
87 present a high degree of spatial and temporal coherence. A simple model of the x-ray imaging with a  
88 coherent beam is useful for the understanding of the physical foundation of the imaging with SR. Using  
89 the wave formalism the plane wave represents a mono-energetic beam travelling in the vacuum given  
90 by:

91 (1)  $\psi = \psi_0 e^{\frac{i2\pi z}{\lambda}} e^{-i\omega t}$

92  $\psi_0$  is the wave amplitude,  $\frac{2\pi}{\lambda} = |k| = k$  is the modulus of the wave vector parallel to the propagation  
 93 direction, here the  $z$  axis. The last term is the time-dependent factor that will be omitted in the  
 94 following equations. For simplicity we will re-write (1) as follows:

95 (2)  $\psi = \psi_0 e^{ikz}$ .

96 If the beam propagates through a homogeneous medium the value of  $k$  in (2) changes to  $k_{\text{medium}} = nk$ .

97 In x-ray physics,  $n$  is usually written as  $n = 1 - \delta + \beta$ .  $\delta$  is the refractive index decrement and  $\beta$  is  
 98 associated to the decrease of the amplitude. Radiographic images are obtained collecting the x-ray  
 99 beam that traversed inhomogeneous samples. The properties of the samples are summarized by the  
 100 refractive index  $n(x, y, z) = 1 - \delta(x, y, z) + \beta(x, y, z)$ . The wave emerging from the sample is the  
 101 result of the product between the incoming radiation and the transmission function,  $T(x, y)$ , of the object  
 102 [6] that depend from the refractive index as follows:

103 (3)  $\psi_{out} = T(xy)\psi_0 e^{ikz}$

104 (4)  $T(x, y) = A(x, y)e^{-i\phi(x, y)}$

105 where

106 (5)  $A(x, y) = e^{-k \int \beta(x, y, z) dz}$

107 (6)  $\phi = -k \int \delta(x, y, z) dz$

108 The beam intensity is equal to squared amplitude of the wave thus the linear attenuation coefficient  $\mu$   
 109 (intensity loss per unit path length) is given by

110 (7)  $\mu(x, y, z) = 2k\beta(x, y, z) = \frac{4\pi}{\lambda}\beta(x, y, z)$ .

111 The physical basis of radiology is the different attenuation of x-rays by different organs of the human  
 112 body. However, attenuation is not the only effect of the sample on the wave. A phase shift,  $\phi$ , is  
 113 associated to the refractive index decrement,  $\delta$ , according to equation (6). The phase shift means that  
 114 the propagation direction of the emerging radiation is modified by the sample, consequently it is no

115 longer a planar wave. The wave vector of the emerging wave,  $k_{out}$ , can be written as in equation (8), if  
116 the spatial derivatives of the wave shift  $\phi(x,y)$  are much smaller than the wave number  $k$

117 (8) 
$$k_{out} = \left( \frac{\partial}{\partial x} \phi(x,y) \right) \hat{x} + \left( \frac{\partial}{\partial y} \phi(x,y) \right) \hat{y} + k \hat{z} \equiv \nabla_{xy} \phi(x,y) + k \hat{z}$$

118 where the xy plane is the object plane. The refraction angle,  $\alpha$ , of the beam emerging from the sample  
119 at the point (x,y) is

120 (9) 
$$\alpha \cong \frac{1}{k} |\nabla_{xy} \phi(x,y)|.$$

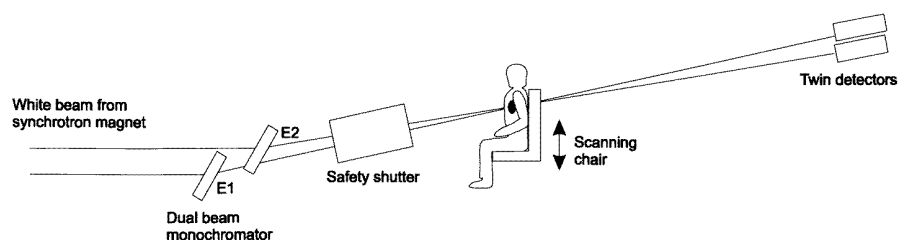
121 One limitation of radiographs is the small contrast the contrast among the soft tissues, i.e. between  
122 cancer and normal tissues or between blood and cardiac muscle. The administration of contrast agents  
123 is a pillar of the modern radiology. The basic idea is to increase the attenuation properties of tissues or  
124 organs where the uptake of the contrast agent is higher. The first generation of in-vivo SR clinical  
125 studies exploited the monochromaticity of the SR beams in presence of a contrast agent [2]. Moreover  
126 new x-ray phase-sensitive imaging techniques have been developed in the last two decades to improve  
127 the image contrast with the contribution of the phase shift term (eq. 6). The application of these  
128 techniques in medical imaging is interesting because in the energy range of the soft tissue x-ray  
129 imaging (15-25 keV)  $\delta$  is reported in the range  $10^{-6}$ - $10^{-7}$  and  $\beta$  is typically 1000 times larger( $10^{-8}$ - $10^{-10}$ )  
130 [7]. The detection of the x-ray refraction requires dedicated techniques because the refraction angle  
131 induced by the biological tissues is of the order of a few microradians.

### 132 3. The medical imaging with SR: the history

#### 133 3.1. The first generation of in-vivo studies: K-edge subtraction imaging

134 The application of SR in clinical radiology started in the 80s with first feasibility studies focused on  
135 coronary angiography. Contrast agents were used to visualize the heart blood arteries [2]. Coronary  
136 angiography studies on patients were carried out at the SR facilities of Brookhaven (USA) [8],  
137 Hamburg (Germany) [9], Tsukuba (Japan) [10] and Grenoble (France) [11]. At that time, the coronary

138 angiography required the patient catheterization of the femoral artery and the arterial injection of  
 139 contrast agent. Hospitalization was required due to the associated risk of haemorrhage. In coronary  
 140 angiography with SR, iodine-based contrast agent was used but it was administered through an  
 141 intravenous injection. It is a less invasive and less risky procedure hence hospitalization was not  
 142 required. The imaging technique developed for this application is the so-called K-edge subtraction  
 143 imaging. Two images are acquired at two monochromatic X-ray energies: the first just below, the  
 144 second just above the K-absorption edge of the contrast agent. From the logarithmic subtraction of  
 145 these images, the visibility of structures perfused by the contrast agent is greatly enhanced and the  
 146 signals due to other tissues are practically suppressed. The idea is simple and elegant and exploits the  
 147 X-ray beam monochromaticity. But since the heart is a moving organ and the subtraction works well  
 148 only if the two images are acquired at the same time to avoid motion artifacts. In order to do this,  
 149 specific monochromators have been developed that create two fan beams at the two optimal energies  
 150 for the k-edge subtraction. The two beams cross themselves in the patient and are detected after the  
 151 patient by two separate linear detectors. In order to acquire the image, the patient is moved in front of  
 152 the beam (Fig. 1) and the images are acquired line-by-line. In the Hamburg protocol, the total  
 153 acquisition time was about 250 ms second for 125 mm scan, the patient velocity was 50 mm/s and the  
 154 pixel size  $\sim 0.4 \text{ mm}^2$  [2].



155  
 156 Figure1: A schematic diagram of the systems used for coronary angiography. (From ref [2], with permission)  
 157

158 The large clinical trial in Hamburg, which included 379 patients, obtained very high specificity  
 159 (99%) and satisfactory sensitivity (79%) for severe stenosis [9]. No complications occurred during or  
 160 after the angiographic procedure and the acceptance by patient was extremely high. No other similar

161 clinical studies have been done in the last decade, probably due to the advent of spiral CT systems and  
162 the development of cardio-CT and angio-CT clinical exams that provided affective tools for low-  
163 invasive and high-quality cardiac imaging in the hospitals [12].

164 At the end of last century, there has been another clinical experience in K-edge subtraction imaging  
165 with SR: a bronchography feasibility study held in Brookhaven with two healthy volunteers by the  
166 inhalation of a xenon (80%) and oxygen (20%) mixture [13]. In analogy with the Magnetic Resonance  
167 Imaging (MRI) studies developed in the same period [14], the idea is to use the xenon signal for  
168 improving the visibility of the bronchial tree. The images were acquired using the same patient chair  
169 developed for the SR coronary angiography. The experiment was successful, planar images were  
170 obtained with a resolution of  $0.5 \times 0.5 \text{ mm}^2$  but it did not meet the interest of the radiological  
171 community. This is probably due to the large diffusion of the new low-dose spiral CT systems in the  
172 same years that allowed tomographic study of the lungs at acceptable delivered dose and cost. The  
173 balance between image quality and delivered dose was so good that CT based screening programs of  
174 lung cancer were evaluated [15, 16]. In the last section of this paper we will discuss of the new interest  
175 in lung imaging with SR.

### 176 3.2. *The advent of phase-contrast x-ray imaging*

177 In section 2.2, the physics of the x-rays refraction has been introduced and the very small value of  
178 refraction angle due to a biological sample has been discussed (a few microradians). This means that  
179 detecting the x-ray refraction induced by the human body during a radiological exam is still a  
180 challenge. The detection of the beam refraction is simplified in case of coherent radiation and therefore  
181 the SR beams are ideal tools for the developments of x-ray phase-sensitive techniques and for their first  
182 applications.

183 A family of phase-sensitive techniques has been developed in the last two decades, each aims to  
184 convert the phase shift into an intensity modulation in order to use it as an additional contrast



185 mechanism in the x-ray image. Following other authors [6,17] they are called propagation-based phase-  
186 contrast imaging (PPCI), analyzer based imaging (ABI), coded apertures phase-contrast x-ray imaging,  
187 interferometry, and grating interferometry (GI). Each technique has appropriate requirements on spatial  
188 and temporal coherence of the radiation and moreover on the spatial resolution of the imaging detector.  
189 Review papers dedicated to these topics have appeared regularly in the scientific literature; probably  
190 the oldest one is by Fitzgerald in 2000 [3]. In references [6,17], recent comprehensive works are also  
191 outlined.

192 In order to be applied in a clinical exam an imaging technique has to match a number of  
193 requirements: acceptable delivered dose, short acquisition time and adequate field of view (FOV).  
194 Moreover the system has to be safe and robust in order to ensure reliable image quality and dose  
195 control in each examination. The PPCI technique meets all these requirements. The position of the  
196 detector is the only difference between absorption-based configuration and PPCI system. A typical  
197 PPCI set-up is summarized in Fig 2b. The first unperturbed wave front  $W_1$  is distorted by the  
198 sample and second wave front  $W_2$  evolve before the signal is recorded by the detector. As a  
199 consequence, a profile with positive as well as negative peaks in correspondence with the detail edges  
200 is visible, increasing low contrast detail visibility. The intensity of the image is proportional to the  
201 Laplacian of the phase-shift calculated with respect to the image plane:  $\nabla_{x,y}^2 \phi(x,y)$  [18]. The main  
202 parameters affecting the PPCI images are the spatial coherence of the beam, the source-to-sample ( $R_1$ )  
203 and the sample-to-detector ( $R_2$ ) distances and the spatial resolution of the detector. The PPCI technique  
204 is also known as “in-line phase-contrast imaging” or “free-space propagation phase-contrast imaging”.

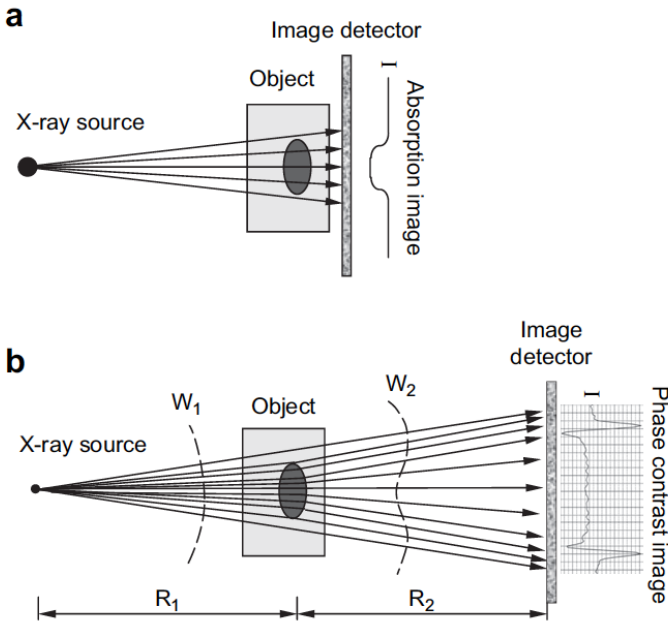


Figure 2: Schemes of (a) an absorption-based imaging configuration and (b) a PPCI configuration from [7], with permission.

In 1995, a paper by Snigirev [19] and co-workers demonstrated that PPCI was feasible with SR. In 1996 Wilkins [18] and co-workers published the images of a small aquarium fish acquired using a microfocus x-ray generator and a film. Due to the difference in geometry between the absorption contrast and the PPCI configurations,  $R_2$  equal to 1 mm and 1.1 m respectively, and the acquisition time increased from 2 minutes to about 2 hours. Two years later the Italian team working at Elettra, the Italian SR facility, published the first images of breast tissue specimens acquired with a mammographic screen-film system and delivering mean glandular doses comparable with doses delivered in clinical practice [20]. This is the prologue of the story of the first clinical study in PPCI that has been took place at the SYRMEP beamline at Elettra.

#### 4. In-vivo phase contrast breast imaging at Elettra

##### 4.1. The SYRMEP beamline at Elettra

When the idea of a European synchrotron radiation facility (ESRF) was under discussion, the proposal to build a SR facility in Trieste was launched during the 71st Annual National Congress of the Italian Physical Society, in October 1985 in Trieste, Italy. Even if Trieste was not selected to be the

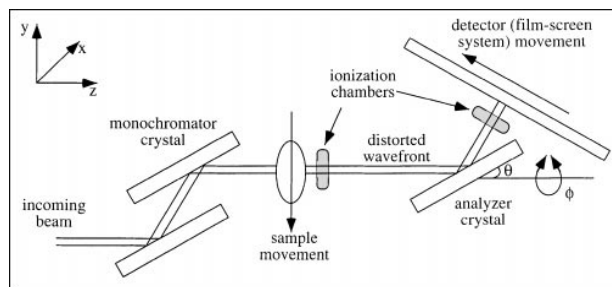
European facility, the project of Elettra, the Italian SR laboratory in Trieste was approved by the national and local institutions. In 1987 the works for design and realization started. Several meetings immediately focused about beamlines to be developed. Medical physicists and radiologists of the University of Trieste were very active in these discussions. The projects about k-edge subtraction coronary angiography were exciting. However the energy spectrum of Elettra was not optimal for such applications. The then chief of the Radiology Department of the University of Trieste, Prof. Ludovico Dalla Palma, indicated mammography as a challenging exam for both radiologists and physicists. The social impact of the breast cancer was evident to everybody and the energy spectrum of Elettra was perfect for mammography. The project for the SYRMEP (SYnchrotron Radiation for MEdical Physics) beamline, already foreseeing the final phase of *in vivo* mammographic examinations, was presented 1991 [21]. As soon as Elettra began its operations in 1993, the construction of the SYRMEP beamline started.

In this story, the dates are important. The SYRMEP project was developed on the basis of the optimization of the mammographic exam in order to obtain the best absorption-contrast image. According to a pilot study done at INFN laboratory of Frascati in 1993 [23], the optimization would be based on an accurate selection of energy of the monochromatic beam and on the high scatter rejection thanks to the laminary cross-section of the beam [22]. The development of a silicon microstrip detector working in single photon counting mode was part of the project [24, 25].

The *in vitro* studies at the SYRMEP beamline started in 1996. In 1995 Snigirev and co-workers published their PPCI results based on SR [19], and in 1996, Wilkins and co-workers published on Nature their famous image of the small fish [18]. Immediately the PPCI set-up was installed at the SYRMEP beamline and with its mission, images of mammographic test objects and of breast specimens were acquired. First results have been published in 1998 [20]. For the first time, the visibility of the PPCI edge-enhancement features has been demonstrated in 3 cm thick human breast sample using mammographic screen-film system. The mammography screen-film systems are

247 characterized by a small dynamic range to obtain high contrast images. If the dose is higher than  
248 expected the film is overexposed and the image is very dark with low contrast, hence not suitable for  
249 radiologic evaluation [26]. The correct exposure of our images was the guarantee of the clinical  
250 delivered dose. In previous works [18,19] on the contrary, the sample thickness was much smaller, the  
251 spatial resolution of the detector was higher and the delivered dose was substantially higher than those  
252 delivered in radiological examination.

253 Immediately a systematic study of full breast samples has been done with a detailed evaluation of the  
254 delivered dose [27]. During this systematic study two phase-sensitive techniques were applied: PPCI  
255 and ABI. In 1997 the team of the medical imaging beamline at the Brookhaven National Laboratory  
256 (USA) published a paper suggesting the possible contribution of ABI to biomedical x-ray imaging [28].  
257 The basic idea was that an analyzer crystal could serve as a very effective antiscattering system, in  
258 analogy with the strictly energy selection done by crystals in the monochromator systems (Fig 3).



259  
260 Figure 3: Schematic depicts the experimental set-up for diffraction imaging measurements. From ref [27] with permission.

261 Nevertheless, by slightly turning the analyzer crystal at different positions additional phase effects  
262 such as refraction, were visible. In Trieste an ABI set-up was immediately developed, using a spare  
263 crystal of the monochromator system. Thanks to the large dimension of the crystal, the FOV of the ABI  
264 system was equal to that of the PPCI. The ABI set-up was not as simple as in PPCI: the required  
265 mechanical stability (within a few microradians) of the analyzer crystal was a problem hence  
266 reproducibility a challenge. Under the radiological point of view, the dose delivered was a little bit  
267 higher than in PPCI and, more important, the images look different from conventional mammography,

268 creating a large enthusiasm from the physicists but prudent comments from the radiologists. On the  
269 contrary, PPCI radiographs obtained the enthusiastic approval of the radiologist because they combine  
270 absorption contrast, PPCI edge-enhancement and a very effective scatter rejection, due to the laminar  
271 beam and the geometric set-up. On the basis of grades assigned by reviewers, image quality of the  
272 PPCI images was demonstrated to be considerably higher than conventional mammography and the  
273 delivered dose fully compatible with clinical studies. The proposal of the clinical mammography study  
274 was developed in close collaboration with the radiologists of the University of Trieste and with the  
275 support of the international scientific committee of Elettra.

#### 276 4.2. *The mammography clinical trial*

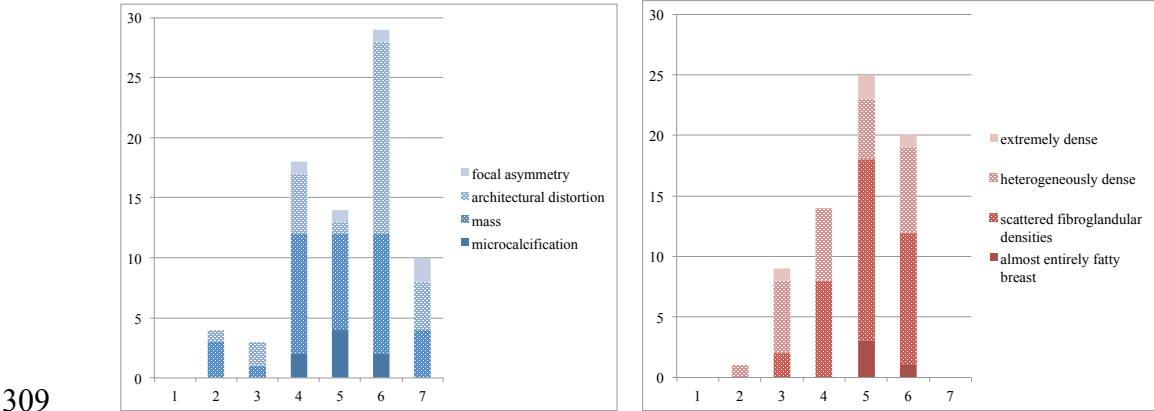
277 The SYRMEP beamline modification phase started in 2000, when the patient room with the patient  
278 scanning support, the control room for radiologists and radiographers, and the control system to comply  
279 with all the dosimetric and safety regulations were designed. In July 2004 the local Ethical Committee  
280 authorized the clinical study and in January 2006, the Ministry of Health gave the ultimate approval.

281 The main characteristics of SYRMEP beamline are: radiation source from a storage ring bending  
282 magnets, a Si(111) double crystal monochromator, beam energy in the range 8.5–38 keV, and energy  
283 bandwidth of the beam  $\frac{\Delta E}{E} = 0.2$ . The beam maximum cross section at the mammography area is 210  
284 mm (horizontal)  $\times$  5 mm (vertical, FWHM). The flux is of the order of  $10^8$  ph/(mm<sup>2</sup> s). A safety and  
285 dosimetric system has been developed for clinical planar mammography [29]. The SYRMEP patient  
286 support allows planar mammography by scanning the compressed breast in vertical direction, and  
287 breast CT acquisition by the rotation of the patient in prone position with the breast hanging at the  
288 rotation centre [30]. The distance between the breast compression system and detector in the PPCI  
289 mammography set-up is 2 m. In order to obtain high quality images merging both absorption and phase  
290 contrast the monochromatic beam energy is selected per each patient according to the following rule: the  
291 lowest energy such that the mean glandular dose (MGD) is less or equal to the one delivered in digital

292 mammography (DM) exam at the hospital. Dose calculations were based on the Boone's Montecarlo  
293 study [31]. The beam energies applied in the mammography exams are in the 17-22 keV range. Thick  
294 breasts required higher energies.

295 Eighty-two patients were selected between March 2006 and May 2012 on the basis of the enrolment  
296 criteria approved by the local ethics committee. In particular, the criteria include patients with an  
297 inconclusive diagnosis after DM and ultrasonography, at the University Hospital of Trieste. The first  
298 study, which included 71 patients, was based on a mammographic screen-film system [32]. Moreover,  
299 a group of 11 patients was studied using a computed radiography (CR) system [33].

300 To evaluate PPCI mammography both image quality and diagnostic results were evaluated. The  
301 image quality analysis was based on the comparative evaluation of the visibility of the breast  
302 abnormalities and of the glandular structure [34]. The employed statistical analysis (Wilcoxon signed-  
303 rank test), highlighted that PPCI mammography depicts normal structures and abnormal findings with  
304 higher image quality with respect to conventional DM (Fig 4). Looking at the different subset of  
305 abnormalities, the statistical tests demonstrated a significant improvement in the visibility of  
306 architectural distortions and masses. Due to the enrollment criteria of the study, only a limited number  
307 of micro-calcifications was acquired and therefore the statistical analysis of this feature is not  
308 significant.



310 Figure 4: Histogram of the scores of relative visibility of breast abnormalities (left) and glandular structure (right). Score of 1: excellent visibility in DM  
311 and poor in PPCI. Score of 2 or 3: visibility of the progressively lower in DM but better than that in PPCI. Score of 4: equal visibility with the two  
312 techniques. Score of 5 or 6: visibility progressively better in PPCI than in DM. Score of 7: excellent visibility in PPCI and poor visibility in DM. From ref  
313 [34] with permission.

314 The diagnosis based on the DM and on the PPCI exams were compared with the gold standard  
315 (biopsy or 1-year follow up) and both PPCI mammography and DM specificities were calculated [32].  
316 A statistically significant increment was observed using PPCI, thus suggesting that PPCI  
317 mammography can be used to clarify cases of questionable or suspicious breast abnormalities identified  
318 at DM. The statistical analysis of the diagnostic performance was affected by the limitations of the  
319 study design. The first is the inclusion criteria recommended by the ethics committee: only patients  
320 with questionable or suspicious abnormalities identified at DM and not clarified by US were included  
321 in the study. This restriction implied that the study population was characterized by a high prevalence  
322 of disease. The second limitation is that the BI-RADS scores were assigned in consensus between two  
323 onsite radiologists, who, due to the study design, read the DM images before referring the patient to  
324 MSR. Thus, they could have been biased in their assessments. However the image quality analysis is  
325 not affected by these limitations and, up to now, this is the only clinical study available. Further studies  
326 are necessary for a better evaluation of the technique. If the positive results will be confirmed the  
327 translation of the PPCI image quality in clinical practice is highly desirable, because this would reduce  
328 the number of additional exams and biopsies. In figure 5 images from a clinical examination are  
329 presented.

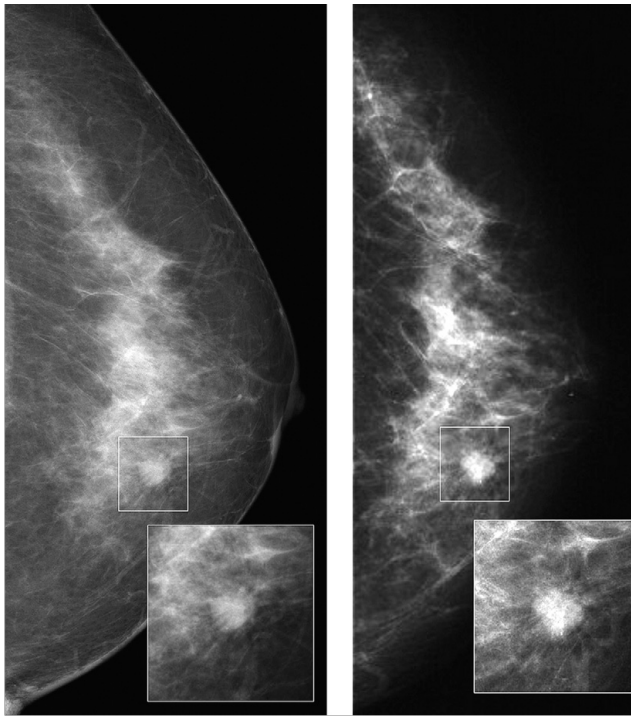


Figure 5: Comparison between (a) digital mammography and (b) PPCI mammography. An equivocal mass is shown enlarged in the insets. In the conventional image, the margins appear partly circumscribed and partly indistinct, leading to an uncertain diagnosis. Conversely, in the PPCI image, the margins result micro-lobulated and partly speculated, indicating a probable breast cancer, as it was later confirmed by histology. Reproduced from ref [35] with permission

The dose evaluation demonstrated that in DM, Entrance Surface Air Kerma (ESAK) increases linearly with breast thickness in the range 2-10 mGy. On the contrary during PPCI exams, ESAK is almost constant (about 2 mGy) for all thickness with a reduction of more than 50% for breast thicker than 4 cm. A significant decrease of the MGD (on average 42%) delivered during PPCI exams compared to DM was also found [36]. These results are obtained using energy selection and exposure optimized for screen-film system. Further dose reductions are possible with digital detectors and higher energy beam. It is well known that digital mammography allows an increase in the beam energy and thus decreases the delivered dose keeping high the image quality, thanks to the increased fluence on the detector [37]. A preliminary study about image quality, beam energy and delivered dose was done using a CR detection system at the SYRMEP beamline [33]. In this study, a mammographic CR system and the mammographic screen-film system were used to acquire PhC images of a breast tissue in the energy range 16-21.5 keV. The same sample was imaged with the DM unit of the University Hospital



348 of Trieste. The blind evaluation of the images by an expert radiologist demonstrated that CR images are  
349 better of the film-screens images for beam energy equal to 19 keV or higher and that all the CR images  
350 are better than the clinical DM images, thanks to the phase-contrast effect. At the same time the air  
351 kerma decreases of about a factor 2 increasing the beam energy from 18.5 keV to 21.5 keV. The  
352 conclusion of this study is that the elevated quality of digital images obtained with SR at high energy  
353 and low dose indicates the possibility of further optimising the clinical use of SR with digital detectors,  
354 which would allow the introduction of more complex techniques including breast CT.

#### 355 4.3. *Direct measurement of breast linear attenuation coefficient*

356 To determine the exposure parameters of each exam, the beam attenuation was evaluated on the  
357 basis of data collected by the ionisation chambers located upstream of the patient, and by a couple of  
358 solid state exposimeters placed in the screen-film system support [34]. From these data, the direct  
359 measurement of the linear attenuation coefficient of the compressed breasts has been done.

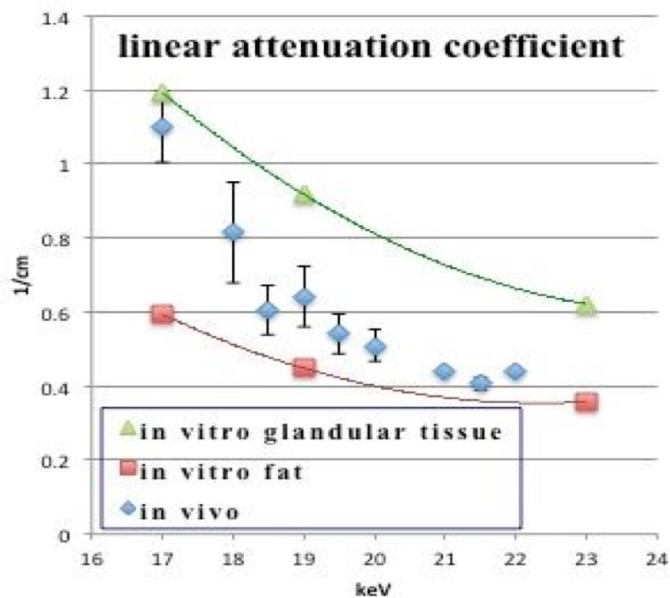
360 Ionisation chambers data has been used for the safety system and for the patient on-line dosimetry,  
361 while exposimeters has been used to evaluate the dose rate at the detector position. The absolute  
362 calibration of ionization chambers was produced in collaboration with the Italian authority for  
363 dosimetry (ENEA) with respect to the primary national standard for air kerma measurements [38]. The  
364 linear attenuation coefficients ( $\mu$ ) obtained in this study are based on the measurements of the beam  
365 intensity before and after attenuation ( $I_0$  and  $I$  respectively) and of the breast thickness ( $x$ ):

$$366 \quad I = I_0 e^{-\mu x} \quad \mu = \frac{1}{x} \ln \frac{I_0}{I}$$

367 The relative calibration between these two systems has allowed the calculation of the ratio ( $I_0/I$ ).  
368 Breast thickness has been obtained from compression paddle position recorded by the control system  
369 and a correction for compression paddle deformation has been included. The pre-exposure has been a  
370 low-dose scan 2 cm long in the central region of the breast and the dimension of the 2 solid state  
371 exposimeters is 2 cm [29], thus the attenuation coefficient is the average value over about 8 cm<sup>2</sup> of

372 compressed breast. The dose delivered during the prescan has been less than 10% of the total exam  
373 dose.

374 The results are summarized in figure 6. The average linear attenuation coefficients are reported in the  
375 energy range 17-22 keV applied in the clinical study. The beam energy selection has been based on the  
376 thickness and the density class of the breast. As discussed in the previous section, the thicker the breast  
377 higher the applied energy. The results obtained have been compared with the linear attenuation  
378 coefficients of glandular and adipose tissues previously measured at the beamline SYRMEP in surgical  
379 samples during a CT study [39].



380

381 Figure 6: Average linear attenuation coefficients of the breast obtained *in vivo* during the PPCI clinical trial. The standard deviations are reported when  
382 more than 3 values were acquired at the same energy. For comparison *in vitro* measurement are presented from ref [39] .

383 For the first time a direct measurement of the linear attenuation coefficient of the breast have been  
384 obtained *in vivo*, thanks to the use of monochromatic radiation in mammography with SR. The values  
385 obtained are intermediate between the linear attenuation coefficients measured *in vitro* for the purely  
386 glandular or adipose tissues during a previous experiment. Despite the considerable and well-known  
387 variability among individuals, it was observed that the thin breasts studied at low energies, have  
388 attenuation values close to those of pure glandular tissue while the thick breasts investigated at higher

389 beam energies demonstrate attenuation properties close to those of adipose tissue. These results may  
390 contribute to a revision of the standard dosimetric breast model that is under discussion in the breast  
391 imaging community [40,41].

#### 392 4.4. *Towards the PhC breast CT clinical study*

393 As discussed in section 3.1 the SYRMEP beamline was designed to perform clinical studies. The  
394 patient support can be rotated in the horizontal plane to acquire the two views of the mammographic  
395 exam. It was also designed to allow the complete rotation of the breast in front of the beam without  
396 artifacts due to rotation. The breast CT was considered from the beginning a “natural” evolution of the  
397 clinical program [30,42] and nowadays the 3D imaging of the breast is the frontier of the breast  
398 imaging in the clinical practice. The new program is called SYRMA-CT (SYnchrotron Radiation  
399 Mammography – Computed Tomography). It involves the INFN (Italian Institute of Nuclear  
400 Physics), Elettra Laboratory and the University Hospital of Trieste. In order to combine high image  
401 quality and low delivered dose a number of innovative elements will be merged: phase retrieval  
402 algorithm, single photon counting detector, and state-of-the-art CT reconstruction algorithms. To  
403 perform an accurate exam optimization, a Montecarlo model has been developed for the dose  
404 calculation based on GEANT4 toolkit [43].

405 The detector selected for this application is PIXIRAD-8, a CdTe detector working in single photon  
406 counting mode (frame rate 20 f/s and 60  $\mu\text{m}$  pixel pitch). The system has a linear response even at  
407  $2 \times 10^5$  photons per pixel per second. The detector is produced by PIXIRAD Imaging counters s.r.l., a  
408 spin-off company of INFN [44,45]. The multi block module used in this project is an 8 unit system  
409 (PIXIRAD-8) reaching a global active area of 250 mm x 25 mm that fits with the beam cross section  
410 (21 cm x 5 mm). This system matches the requirements for SYRMA-CT project in terms of active area,  
411 frame rate and linearity. Moreover direct detection by 0.65 mm thick layers of CdTe allows high  
412 detection efficiency and minimizes the loss of spatial resolution due to blurring of light in scintillator-

413 based systems. The spatial resolution of the detector is a crucial in PPCI because the detection of the  
414 edge-enhancement features is necessary.

415 The aim of the project is to acquire tomographic images of the breast delivering MGDs in the range  
416 of doses delivered at the Cone Beam Breast CT prototypes (4-20 mGy) or lower [46]. The beam energy  
417 will be in the range 35-40 keV, the upper limit is determined by the beam available at the SYRMEP  
418 beamline and it is a compromise between dose optimization [47] and Elettra energy spectrum. To  
419 obtain low-dose high-quality CT images, several approaches have been proposed dealing with the  
420 reduced number of projections problem, including iterative and algebraic techniques [48], some of  
421 them were applied to breast CT [49,50,51]. A comparative analysis of their performance in SYRMA-  
422 CT experimental condition is on going. Moreover the phase contrast information embedded in the data  
423 will be exploited applying a phase retrieval filter [52] before the actual tomographic reconstruction in  
424 order to increase the image contrast [53].

425 The protocol of the breast CT exam is under discussion considering the peculiar set-up. There are a  
426 number of issues under evaluation: such as the number of slices to be acquired and the total acquisition  
427 time. The vertical beam size at the breast is about 3 mm, which means that to investigate a volume of 3  
428 cm thickness in the thorax-nipple direction 10 acquisitions are necessary in 10 vertical positions of  
429 patient support. In analogy with MRI exams, we are planning a total examination time of 10 minutes or  
430 shorter, without breast compression and with a comfortable breast immobilizer system. The dose  
431 delivered to the investigated volume will be comparable with a two views mammography and  
432 comparable or smaller than the dose delivered at the cone beam breast CT prototypes. Based on our  
433 experience the continuous multiple rotations of the support are rather acceptable for the patients.

434 Preliminary images on test objects and breast tissue samples have been acquired and the image  
435 processing work is on going.

## 436 5. Future trends

437 Apart from mammography, new clinical trials are expected at SR facilities in the future. A number of  
438 beamlines designed for bio-medical researches are suitable for *in vivo* studies, based on the beam size,  
439 flux, energy range and patient support technologies [6]. Two emerging applications will be briefly  
440 discussed: lung imaging and imaging for SR radiation therapy.

### 441 5.1. Clinical interest of lung imaging with SR

442 PPCI was applied to lung imaging in animals with promising results: the multiple x-ray refraction in  
443 the alveoli creates a speckled intensity pattern that is related to the airway morphology [54]. *In vivo*  
444 PPCI investigations of the process of lung clearance in newborn rabbit pups, including optimization of  
445 mechanical ventilation, obtained significant results with important implication for clinical practice [55].  
446 The use of PPCI in lung has great potential in the early diagnosis of subtle, and no uniform lung  
447 diseases. *In vivo* mouse models of cystic fibrosis PPCI allowed the study of airway surfaces and lumen  
448 characteristics [56] and the tracking the motion of individual speckles was used as an approximate  
449 model of lung tissue displacement [57].

450 The K-edge subtraction imaging of the lung has been recently extended to CT imaging. The  
451 technique is based on the k-edge of the xenon, thanks to the inhalation of a mixture of xenon and  
452 oxygen by the investigated subject as discussed in section 3.1. Even if no clinical program in lung  
453 imaging with SR is under development, some preliminary dose evaluations have been recently  
454 published for *in vivo* k-edge subtraction CT of the lung [58], considering a possible extension of this  
455 technique in humans, especially for early diagnosis of lung diseases in children.

### 456 5.2. Imaging for the clinical studies in SR radiation therapy

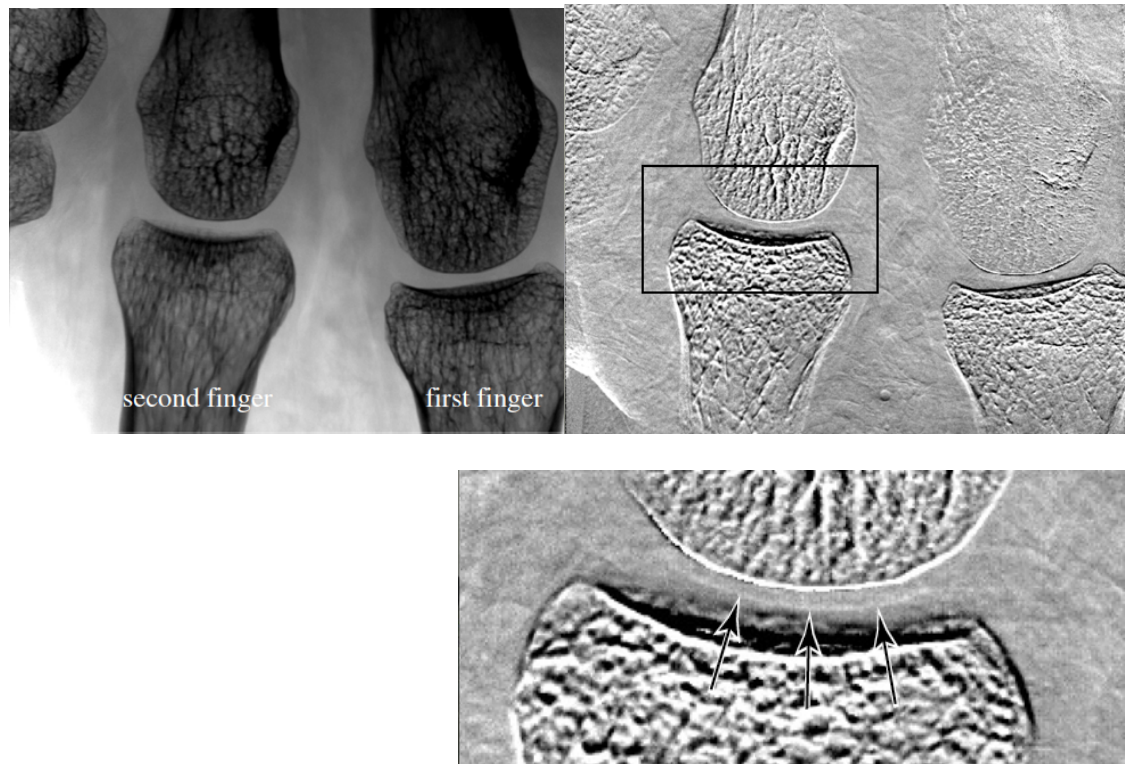
457 A family of innovative and promising techniques for radiation therapy are under development and  
458 testing at SR laboratories: the Synchrotron Stereotactic Radiation Therapy (SSRT) and the Microbeam

459 Radiation Therapy (MRT) [59]. The SSRT is already in its clinical trial stage at the European  
460 Synchrotron Radiation Facility (ESRF) in France [60].

461 In radiation therapy, the correct positioning of the region to be irradiated in the beam is a crucial step  
462 of the protocol. Portal imaging is the acquisition of images using a therapeutic beam to form an image  
463 of the area that is being irradiated. Preliminary study in animals has been done at SPring-8 (Japan) in  
464 order to evaluate the image quality of PPCI using a SR white beam suitable for radiation therapy  
465 (average energy 130 keV) [61]. The results indicate that PPCI portal images represent the head  
466 anatomy in detail and that they can be used for localization of the volume to be treated and for  
467 verification of the treatment.

### 468 5.3. *The translation to the hospitals*

469 Generally speaking, two strategies are possible in order to perform phase-contrast imaging or the k-  
470 edge subtraction imaging at the hospitals: the application of these techniques with conventional x-ray  
471 tubes or the development of a new generation of x-ray sources. Recently a clinical prototype of a  
472 grating interferometry system was developed in Japan, based on a conventional x-ray tube [62]. The  
473 system is used for cartilage studies and the images of one of the authors' palm were published (Fig 7):  
474 the field of view is  $49 \times 49 \text{ mm}^2$ , acquisition time is 32 s, including 19 s of irradiation time, and the skin  
475 dose is about 5 mGy. Small motion artefacts are visible, due to the relatively long acquisition time and  
476 the multiple images necessary for this technique. Increasing the field of view will be a technical  
477 challenge and the training of the radiologists, who are not familiar with the differential phase images,  
478 will be necessary [1], nevertheless here we are at a milestone of our story from the Mrs. Roentgen's  
479 hand to the Prof. Momose's palm via the SR imaging and the phase-contrast techniques.



480

481

482 Figure7: *in vivo* palm images obtained with a GI system: absorption image (top left), differential phase image (top right) and its zoomed image at the  
 483 rectangle indicated (bottom). Cartilage in a joint is revealed as indicated by the arrows. X-ray refraction in the vertical direction of the images is sensed.  
 484 From ref [1] with permission.

485 Grating interferometry [63] is not the only phase-sensitive technique candidate for the development  
 486 of clinical units based on conventional x-ray tube. Coded aperture (or edge illumination) technique is  
 487 another promising approach [64] that is under development at University College of London after a  
 488 pilot study at SYRMEP beamline long time ago [65]. An attempt was done with the ABI system, but a  
 489 lack of intensity of about 1 order of magnitude of the x-ray tube and the unusual contrast of the images  
 490 prevent the development of a clinical prototype [66,67].

491 In principle, the k-edge subtraction imaging is feasible using a conventional x-ray tube and a single  
 492 photon counting detector with multiple thresholds. This approach is called also “spectral imaging”.  
 493 Preliminary spectral imaging CT results are very promising [68], and recently first images obtained  
 494 with a whole-body photon-counting CT system have been presented [69].

495 The research for new x-ray sources is a fascinating field. A number prototypes based on different  
 496 technologies are under development and evaluation (ie electron-impact liquid-metal-jet, Thomson

497 backscattering). The reader will find a summary about the coherent x-ray sources in ref [6] and a  
498 comprehensive discussion can be found in ref [70]. As reported in the introduction the performance of  
499 a source for clinical radiology is quite demanding in terms of flux and focal spot. It is hard to predict  
500 when a new generation of x-ray source will be in use in radiological departments.

## 501 **6. Conclusions**

502 Synchrotron radiation is an ideal x-ray source for imaging and a large number of interesting  
503 scientific cases take advantages of its properties. Its application to medical imaging allowed the  
504 development of powerful and promising techniques as phase-contrast imaging and k-edge subtraction  
505 imaging. A limited number of clinical studies have been done at SR facilities and a new one in phase-  
506 contrast breast CT is under development at Elettra (Trieste, Italy).

507 In clinical practice, the radiological techniques have to work at the hospitals with clinical systems  
508 that are easy to use and at acceptable costs. However the translational research from the laboratories to  
509 the hospital requires a large amount of effort and funds. In this perspective, the clinical trials at the SR  
510 facilities are important in order to evaluate the clinical impact of the new technologies and motivate  
511 further researches towards new instrumentation suitable for diagnostic imaging departments.

## 512 **Acknowledgments**

513 The pioneering roles of the retired Professors Edoardo Castelli and Ludovico Dalla Palma, a  
514 physicist and a radiologist, respectively, are duly recognized.

515 The author is indebted to all the collaborators of the SYRMA-CT project and thanks Frances C.  
516 Lopez, PhD, for the careful revision of the manuscript.

517 The mammography facility at the SYRMEP was built on the basis of a CRTrieste grant.

518



## 519    **References**

- 520    [1] A. Momose, W. Yashiro, K. Kido, J. Kiyohara, C. Makifuchi, T. Ito, S. Nagatsuka, C. Honda, D. Noda, T. Hattori, T. Endo, M. Nagashima and J.  
521    Tanaka *Phil. Trans. R. Soc. A* 372 (2014) 20130023.
- 522    [2] R. Lewis *Phys. Med. Biol.* 42 (1997) 1213–1243.
- 523    [3] R. Fitzgerald *Phys. Today* June (2000) 23.
- 524    [4] S. Mobilio, F. Boscherini, C. Meneghini (Eds), *Synchrotron Radiation Basics, Methods and Applications*, Springer-Verlag Berlin Heidelberg 2015
- 525    [5] McMorro D and Als-Nielsen J *Elements of Modern X-Ray Physics* 2nd edn. (2011) John Wiley & Sons. Singapore
- 526    [6] Rigon L. (2014) In: Brahme A. (Editor in Chief.) *Comprehensive Biomedical Physics*, vol. 2, pp. 193-220. Amsterdam: Elsevier.
- 527    [7] S.-A. Zhou and A. Brahme *Physica Medica* 24 (2008) 129
- 528    [8] W. Thomlinson, in: E Burattini and A Balerna (Eds) *Biomedical Applications of Synchrotron Radiation* 1995 IOS, Amsterdam
- 529    [9] W.-R. Dix, W. Kupper, T. Dill, C. W. Hamm, H. Job, M. Lohmann, B. Reime and R. Ventura *J. Synchrotron Rad.* 10 (2003) 219-227
- 530    [10] Ohtsuka S, Sugishita Y, Takeda T, Itai Y, Tada J and Hyodo K *Br. J. Radiol.* 72 (1999) 24
- 531    [11] H Elleaume, S Fiedler, F Esteve, et al *Phys. Med. Biol.* 45 (2000) L39
- 532    [12] J. Rodenwaldt *Eur Radiol* 13 (2003) 748
- 533    [13] J.C. Giacomini, H. Gordon, R. O’Neil et al *NIM A* 406 (1998) 473
- 534    [14] H.E. Moller, X.J. Chen, B. Saam, K.D. Hagspiel, G.A. Johnson, T.A. Altes, E.E. de Lange and H.-U. Kauczor *Magnetic Resonance in Medicine*  
535    47:1029–1051 (2002)
- 536    [15] T. Nawa, T. Nakagawa, S. Kusano, Y. Kawasaki, Y. Sugawara and H. Nakata *Chest* 122 (2002) 15
- 537    [16] J.R.C. Ellis and F.V. Gleeson *British Journal of Radiology* 74 (2001) 882
- 538    [17] A. Bravin, P. Coan and P. Suortti *Phys. Med. Biol.* 58 (2013) R1
- 539    [18] Wilkins SW, Gureyev TE, Gao D, Pogany A, Stevenson AW. *Nature* 384 (1996) 335
- 540    [19] Snigirev A, Snigireva I, Kohn V, Kuznetsov S, Schelokov I. *Rev Sci Instrum* 66 (1995) 5486
- 541    [20] Arfelli F, Assante M, Bonvicini V, Cantatore G, Castelli E, Palma LD, et al. *Phys Med Biol* 43 (1998) 2845
- 542    [21] E. Castelli, F. Arfelli, D. Dreossi, R. Longo, T. Rokvic, M.A. Cova, E. Quaia, M. Tonutti, F. Zanconati, A. Abrami, V. Chenda, R.H.Menk, E. Quai,  
543    G. Tromba, P. Bregant, F. de Guarrini *NIMA* 572 (2007) 237–240
- 544    [22] Arfelli F, Barbiellini G, Bonvicini V., Bravin A., Cantatore, G., Castelli, E., Dalla Palma, L., Di Michiel M., Longo R., Olivo A., Pani S., Pontoni D.,  
545    Poropat P., Prest M., Richter, G., Rosei R., Sessa M., Tromba G., Turchetta R., Vacchi A. *Physica Medica* 13 SUPPL.1 (1997)7
- 546    [23] E. Burattini, E. Cossu, C. Di Maggio, M. Gambaccini, P.L. Indovina, M. Marziani, M. Pocek, S. Simeoni, G. Simonetti *Radiology* 195 (1995) 239
- 547    [24] Arfelli, F., Bonvicini V., Bravin, A. et al *Physics in Medicine and Biology* 42 (1997) 1565
- 548    [25] Arfelli, F., Bonvicini V., Bravin, A. et al *Radiology* 208 (1998) 709
- 549    [26] M. Mahesh *RadioGraphics* 2004; 24:1747–1760
- 550    [27] F. Arfelli, V. Bonvicini, A. Bravin et al *Radiology* 215 (2000) 286
- 551    [28] Chapman D, Thomlinson W, Johnston RE, Washburn D, Pisano E, Gmur N, et al. *Phys Med Biol* 42 (1997) 2015.
- 552    [29] Longo R , Abrami A , Arfelli F et al. In: Hsieh J, Flynn MJ, eds. *Proceedings of SPIE: medical imaging 2007—Physics of medical Imaging*. Vol  
553    6510, 65100T. Bellingham, Wash : International Society for Optical Engineering , 2007
- 554    [30] S. Pani, R. Longo, D. Dreossi et al. *Phys. Med. Biol.* 49 (2004) 1739

555 [31] JM Boone Med Phys 29 (2002) 869

556 [32] E. Castelli, M. Tonutti, F. Arfelli et al. Radiology 259 (2011) 684

557 [33] E. Quai, R. Longo, F. Zanconati et al Radiol Med 118 (2013) 89

558 [34] R. Longo, M. Tonutti, R. Rigon et al Phil. Trans. R. Soc. A 372 (2014) 20130025

559 [35] D. Dreossi D, A, Abrami, A. Arfelli et al. European Journal of Radiology 68 (2008) S58

560 [36] C. Fedon, E. Quai, F. Arfelli et al ECR 2014/C-1253 (<http://dx.doi.org/10.1594/ecr2014/C-1253>)

561 [37] P. Oliva, B. Golosio, S. Stumbo et al. Med. Phys. 36 (2009) 5149

562 [38] Bovi M , Laitano RF , Pimpinella M , et al . Proceedings of the Absorbed Dose and Air Kerma Primary Standards, Paris, France, May 9–11, 2007.  
563 [http://www.nucleide.org/ADAKPS\\_WS/Session%20G%20-%20Special%20Standards/G4\\_Pa-Toni.pdf](http://www.nucleide.org/ADAKPS_WS/Session%20G%20-%20Special%20Standards/G4_Pa-Toni.pdf) . Published October 2, 2007. Accessed July  
564 26, 2015.

565 [39] RC Chen, R. Longo, L. Rigon et al Phys. Med. Biol. 55 (2010) 4993

566 [40] M. J. Yaffé, J. M. Boone, N. Packard et al Med. Phys. 36 (2009) 5437

567 [41] S. Vedantham, L. Shi, A. Karellas and A.M. O’Connell Med. Phys. 39 (2012) 7317

568 [42] L. Rigon, F. Tapete, D. Dreossi et al. NIMA 628 (2011) 419

569 [43] C. Fedon, F. Longo, G. Mettievier, R. Longo Phys Med Biol 60 (2015) N311–N323

570 [44] Bellazzini R, Spandre G, Brez A, Minuti M, Pinchera M and Mozzo P J Instrum 8 (2013) C02028

571 [45] Vincenzi A, De Ruvo P L, Delogu P, Bellazzini R, Brez A, Minuti M, Pinchera M, Spandre G J Instrum 10 (2015) C04010

572 [46] Vedantham S, Shi L, Karellas A , O’Connell A M and Conover D L Phys. Med. Biol. 58 (2013) 7921

573 [47] Mittone A, Bravin A, Coan P Phys Med Biol 59 (2014) 2199

574 [48] M. Beister, D. Kolditz and W. A. Kalender Physica Medica 28 (2012) 94

575 [49] A. Makeev and S.J. Glick Med. Phys. 40 (2013) 081904

576 [50] Bian J, Yang K, Boone J M, Han X, Sidky E Y and Pan X Phys. Med. Biol. 59 (2014) 2659

577 [51] Y. Zhao, E. Brun, P. Coan et al. Proc. Natl. Acad. Sci. USA 109 (2012) 18290

578 [52] Paganin D, Mayo SC, Gureyev TE, Miller PR and Wilkins SW. J. Microsc (2002) 206 33-40

579 [53] Gureyev T E et al. J. Phys. D: Appl. Phys. 47 (2014) 365401

580 [54] M.J. Kitchen, D. Paganin, R.A. Lewis, N. Yagi, K. Uesugi and S.T. Mudie Phys Med Biol 49 (2004) 4335

581 [55] Kitchen MJ, Paganin DM, Uesugi K, et al. Optics Express 18 (2010) 19994

582 [56] KKW Siu, KS Morgan, DM Paganin, et al. European Journal of Radiology 68 (2008) S22.

583 [57] A. Fouras, BJ Allison, MJ Kitchen et al. Annals of Biomedical Engineering 40 (2012) 1160.

584 [58] S. Strengell, J. Keyrilainen, P. Suortti, S. Bayat, A. R. A. Sovijarvid and L. Porra J. Synchrotron Rad. 21 (2014) 1305

585 [59] E. Brauer-Krisch et al. Physica Medica 31 (2015) 568

586 [60] Y. Prezado, J.F. Adam, P. Berkvens et al AIP Conference Proceedings 1266 (2010) 101

587 [61] K. Umetani and T. Kondoh Review of Scientific Instruments 85 (2014) 073704

588 [62] J. Tanaka<sup>1</sup>, M. Nagashima, K. Kido, Y. Hoshino, J. Kiyohara, C. Makifuchi, S. Nishino, S. Nagatsuka, A. Momose Zeitschrift für Medizinische  
589 Physik 23 (2013) 222

590 [63] F. Pfeiffer, T. Weitkamp, O. Bunk and C. David Nature Physics 2 (2006) 258

591 [64] A. Olivo, S. Gkoumas, M. Endrizzi et al Med. Phys. 40 (2013) 090701-1

- 592 [65] A. Olivo, F. Arfelli, G. Cantatore, R. Longo, R. H. Menk, S. Pani, M. Prest, P. Poropat, L. Rigon, G. Tromba, E. Vallazza, and E. Castelli Med. Phys.  
593 28 (2001)1610
- 594 [66] C. Parham, Z. Zhong, D.M. Connor, D. Chapman, E. D. Pisano Acad Radiol 16 (2009) 911
- 595 [67] L. Faulconer, C. Parham, D. M. Connor, Z. Zhong, E. Kim, D. Zeng, C. Livasy, E. Cole, C. Kuzmiak, M. Koomen, D. Pavic, E. Pisano Acad Radiol.  
596 16 (2009) 1329
- 597 [68] Schlomka et al Phys. Med. Biol. 53 (2008) 4031
- 598 [69] Z. Yu, S. Leng, S. M. Jorgensen, Z. Li, R. Gutjahr, B. Chen, X. Duan, A. F. Halaweish, L. Yu, E. L. Ritman, C. H. McCollough Proc. SPIE 9412,  
599 Medical Imaging 2015: Physics of Medical Imaging, 94120W (doi: 10.1117/12.2082739)
- 600 [70] M. Uesaka and M. Danielsson Eds (Brahme A. Editor in Chief) Comprehensive Biomedical Physics, vol. 8